Separation Science and Technology
Publication details, including instructions for authors and subscription information:
http://www.informaworld.com/smpp/title~content=t713708471

Microfiltration and Ultrafiltration As a Pretreatment For Nanofiltration of Surface Water

Sangho Lee[a]; Chung-Hak Lee[b]
[a] Korea Institute of Construction Technology, Gyeonggi-Do, South Korea [b] School of Chemical Engineering, Seoul National University, Seoul, Korea

To cite this Article Lee, Sangho and Lee, Chung-Hak(2006) 'Microfiltration and Ultrafiltration As a Pretreatment For Nanofiltration of Surface Water', Separation Science and Technology, 41: 1, 1 — 23
To link to this Article: DOI: 10.1080/01496390500446426
URL: http://dx.doi.org/10.1080/01496390500446426

Separation Science and Technology, 41: 1–23, 2006

ISSN 0149-6395 print/1520-5754 online
DOI: 10.1080/01496390500446426

Microfiltration and Ultrafiltration As a Pretreatment For Nanofiltration of Surface Water

Sangho Lee
Korea Institute of Construction Technology, Gyeonggi-Do, South Korea

Chung-Hak Lee
School of Chemical Engineering, Seoul National University, Seoul, Korea

Abstract: The efficiency of pretreatment using microfiltration (MF) and ultrafiltration (UF) was investigated in surface water nanofiltration for drinking water production. A series of pretreatments prior to NF were performed to examine their efficiency to improve NF flux. Based on lab-scale nanofiltration experiments, the major foulants appeared to be colloidal particles rather than dissolved organic matter for surface water containing hydrophilic organics. During the NF operations, changes in particle size by MF/UF pretreatment were found to be the reason for different pretreatment efficiencies with the pore size of prefilters. NF flux and pretreatment efficiency were quantitatively interpreted using a theoretical approach based on the particle back-transport model. Considering the energy consumption to produce unit volume of NF permeate, optimum pretreatment conditions were suggested.

Keywords: Microfiltration, ultrafiltration, surface water pretreatment, nanofiltration

INTRODUCTION

The more rigorous regulation of water quality and a decrease in the amount of adequate water sources have led to an increased interest in applying nanofiltration (NF) for drinking water production. In addition to removing virtually all

Received 22 February 2005, Accepted 20 October 2005
Address correspondence to Prof. Chung-Hak Lee, School of Chemical Engineering, Seoul National University, Seoul 151-744, Korea. Tel.: 82-2-874-0897; Fax: 82-2-874-0896; E-mail: leech@snu.ac.kr

particles, the NF process rejects significant amounts of soluble organic species (1) and therefore presents a technology with the potential to remove disinfection by-product precursors from ground and surface water (2). However, problems related to a decline in flux and membrane fouling poses limitations to the acceptance and use of NF for drinking water production.

Factors affecting NF fouling have been studied, including membrane properties and major foulants in feed water. The hydrophilic cellulose acetate membranes exhibited a greater flux than hydrophobic thin film composite membranes because of smaller surface interaction between foulants and membrane surfaces (3). With respect to fouling materials, several studies have demonstrated that dissolved organic matters (DOM), mainly humic and fulvic acid, play a key role in NF flux decline (4–7). However, other studies on the water containing low concentration of DOM have showed that the influence of colloidal particles is more important (8–10).

The most practical way to improve NF flux is to treat raw water prior to NF. This is because it is difficult to dislodge the foulants from a NF membrane and recover the flux to the original level once fouling occurs. Accordingly various attempts to develop proper pretreatment processes have been made including coagulation (11), GAC adsorption (12), ozonation (13), chlorination (14), dissolve air floatation (15) and MF/UF prefiltration, etc. However, conventional treatments such as coagulation and sedimentation were not adequate in preventing NF fouling in many cases (16). On the other hand, MF and UF have proved to be attractive methods for the pretreatment of NF feed water (17, 18). Compared to conventional pretreatments, membrane-based pretreatment exhibited a higher NF flux (19).

Previous works mainly focused on the applications of MF/UF for NF pretreatment in case studies (18, 20, 21) but little information is available on the quantitative analysis of MF/UF pretreatment and the correlation between the prefilter pore size and the extent of flux improvement in surface water NF. Moreover, it is of practical importance to establish general rules concerning the optimum selection of pretreatment for NF using MF/UF.

The purpose of this study was to evaluate the efficiency of pretreatment using MF/UF in surface water NF for different fluid velocities and prefilter pore sizes. A theoretical interpretation of pretreatment efficiency was attempted based on hydrodynamic particle transport model. A quantitative comparison among various MF/UF pretreatments was conducted based on specific energy consumption for pretreatment and NF.

THEORY

Mechanisms of Particle Transport in Crossflow Membrane System

In a crossflow membrane, particle transport depends on two major actions: one action of which is moving the particles toward the membrane surface

(negative direction) and the other involves shifting them away from the membrane surface (positive direction). The negative direction forces include van der Waals attraction (F_A), and permeation drag (F_d), while the positive direction actions include electrical double layer repulsion (F_R), Brownian diffusion (F_B), shear-induced diffusion (F_s), and lateral inertial lift (F_l). The gravity and buoyancy forces are equal to zero assuming that the density of particle is the same as that of the flowing liquid. The rate of momentum of a particle equals the sum of all the forces imposed on the particles in a fluid stream along a membrane channel. Thus the net force exerted on a particle along the membrane channel, F, is the sum of all forces noted above.

$$F = \frac{\pi}{6} d_p^3 \rho_p \frac{dv_p}{dt} = (F_R - F_A) + (F_B + F_s + F_l) - F_d \tag{1}$$

where d_p is the particle diameter; ρ_p is the density of particle; and v_p is the particle transport velocity.

Dividing Eq. (3) by $3\pi\eta d_p$, the particle transport equation can be transformed into the form composed of corresponding velocities.

$$\frac{1}{18} \frac{d_p^2 \rho_p}{\eta} \frac{dv_p}{dt} = (v_R - v_A) + (v_B + v_s + v_l) - J \tag{2}$$

where η is the dynamic viscosity of the feed; v_A is the velocity induced by van der Waals attraction; v_R is the velocity induced by electrical double layer repulsion; v_B is the Brownian diffusion velocity (F_B); v_s is the shear-induced diffusion velocity; v_l is the lateral inertial lift velocity; J is the permeate flux. At a steady state ($dv_p/dt = 0$) the above equation can be simplified to:

$$J_{ss} = v_i + (v_B + v_s + v_l) \tag{3}$$
$$\text{(a)} \qquad \text{(b)}$$

where v_i is the interaction induced migration velocity and can be expressed as a difference between repulsive and attractive interaction ($v_R - v_A$). J_{ss} is the steady state flux, which is governed by surface interaction migrations (a) and hydrodynamic back-transport (b). Each of the back-transport velocities may be calculated as the following equations (22, 23):

$$v_i = \frac{D_B}{\delta} \ln\left(\frac{V_B}{\delta}\right) \tag{4}$$

$$v_B = \frac{0.807 D_B^{2/3} \gamma_w^{1/3}}{L^{1/3}} \ln\left(\frac{C_w}{C_b}\right) \tag{5}$$

$$v_s = \frac{0.807 D_s^{2/3} \gamma_w^{1/3}}{L^{1/3}} \ln\left(\frac{C_w}{C_b}\right) \tag{6}$$

$$v_l = 0.577 \frac{r_p^3 U_m^2}{l^2 \nu} \tag{7}$$

where D_B represents the Brownian diffusion coefficient ($=k_B T/6\pi\mu r_p^2$); D_s the shear-induced diffusion coefficient ($=0.03\ r_p^2\gamma_w$); V_B the potential barrier, δ the boundary layer thickness; γ_w the shear rate; C_w the particle concentration at membrane surface; C_b the particle concentration at bulk solution; L the membrane length; l the channel height; ν the kinematic viscosity of the dispersing medium; U_m the maximum flow velocity at channel entrance; r_p the radius of particle. Equation (7) is the maximum lift velocity at the dimensionless distance of 0.6 from the wall (24, 25). The boundary layer thickness was obtained by Leveque's equation:

$$\frac{d_h}{\delta} = 1.62[\mathrm{Re} \cdot Sc \cdot (d_h/L)]^{1/3} \tag{8}$$

where d_h is the hydraulic diameter of channel entrance. Thus the steady state flux can be estimated from Eqn (3) since the steady state flux corresponds to the critical flux at which no additional particle deposition takes place with time.

Energy Consumption in a Membrane Filtration System

The pumping power (E) required to push an incompressible fluid can be expressed by the difference in power between the inlet and outlet of a membrane module, and these can be calculated by multiplying the volumetric flow rate by the pressure.

$$E = Q_i \times P_i - Q_c \times P_c - Q_p \times P_p \tag{9}$$

where Q_i, Q_c and Q_p are the flow rate at the inlet, concentrate, and permeate line of the membrane module and P_i, P_c, and P_p are the pressures at the inlet, concentrate, and permeate, respectively (Fig. 1). Since pressures at the outlet and permeate of a membrane module are atmospheric, the applied power can be stated as

$$E = Q_i \times \Delta P_i = u_i \times S \times \Delta P_i \tag{10}$$

where ΔP_i is the difference between inlet and atmospheric pressure; u_i the crossflow velocity in membrane module; S the cross section area of membrane flow channel. The energy used can be obtained by integrating the power over time and the amount of total permeate can be obtained by integrating the permeate flow rate by the total operation time (t_t). Thus, the

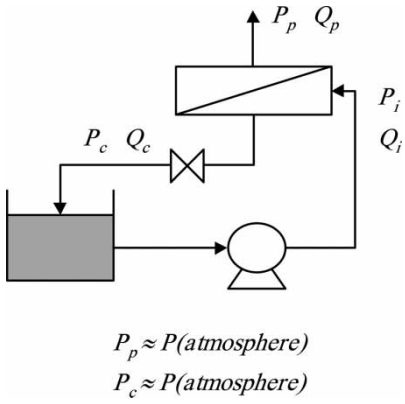

Figure 1. Open recycle membrane filtration loop.

specific energy defined as the amount of energy consumption to produce the unit volume of permeate is calculated using the equation below.

$$W = \frac{\int_0^{t_t} Edt}{\int_0^{t_t} Q_p dt} = \frac{\int_0^{t_t} u_i \times S \times \Delta P_i dt}{\int_0^{t_t} J \times A dt} \tag{11}$$

where A is the membrane area.

MATERIALS AND METHODS

System Operation

The configuration of the experimental apparatus with a cross-flow filtration is shown in Fig. 2. The system consists of a feed tank with a total working volume of 20 L, a diaphragm pump for the recirculation of retentate and a nanofiltration (NF) unit. The membranes used were FilmTec NF-45 polyamide membranes with a salt rejection of 40% for NaCl, tested at 2,000 mg/L feed concentration. The rejection for divalent ions by NF-45 was over 95%. A plate-and-frame membrane module was used with a width 25 mm, a channel length of 110 mm and a channel height of 1.3 mm, respectively. The transmembrane pressure inside the module was regulated to 10 bar using the back pressure valve. The fluid velocity through the membrane channel was adjusted by controlling the speed of the pump motor with an electrical inverter (Goldstar Starverter-G, Korea). The retentate and permeate from the NF loop were returned to the feed tank to maintain a constant working. The Permeate was collected in a reservoir on the electronic balance and the data was collected on a personal computer. The feed water was maintained at a temperature of 25°C by a water jacket in order to minimize the effect of temperature on the filtration results.

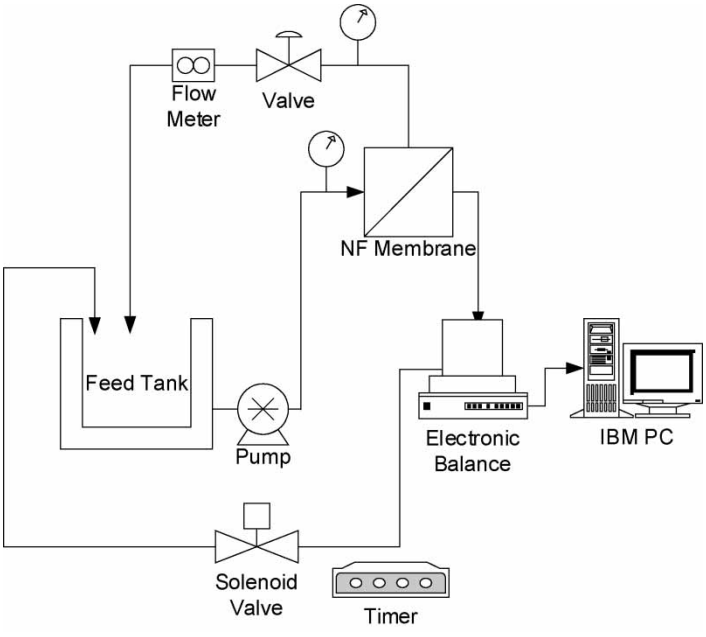

Figure 2. Schematic diagram of experimental device.

The raw water was taken from the Han River in Korea. The water composition is shown in Table 1. Since the experiments were conducted using real surface water, water qualities slightly varied every time the samples were collected from the river. There are small differences among the water qualities of samples in same feed water. Nevertheless, the variations appear to be small as indicated in Table 1.

Analytical Methods

TOC, ion concentration, and suspended solid contents for raw water and membrane permeate were analyzed using the procedures described in the Standard method (26). Particle size and the distribution of solids present in the feed water and retentate were measured using a light scattering instrument (Malvern MasterSizer/E, UK). The zeta potential of solids in the feed water was analyzed with a zeta potential analyzer (Coulter Delsa 440SX, U.S.A).

SDI and MFI

The silt density index (SDI) test was carried out by passing feed water through a 0.45 μm microfilter in a dead end mode at a constant pressure and

Table 1. Raw water composition

	Minimum	Maximum	Average
SS(mg/L)	3.5	7.5	5.5
Turbidity(NTU)	2.0	9.0	5.0
TOC(mg/L)	1.5	3.1	2.3
$UV_{254}(cm^{-1})$	0.023	0.053	0.043
$SUVA(L/mg^{-m})$	1.5	1.8	1.7
THMFP (μg/L)	66	72	70
HPC(CFU/100 mL)	4.0×10^4	6.0×10^4	5.0×10^4
Ca(mg/L)	10	20	10.5
Mg(mg/L)	3	4	3.3
Fe(mg/L)	0.0	0.06	0.05
Mn(mg/L)	0.0	0.02	0.01
Average zeta potential (mV)	−9.5	−11.3	−10

determining the filter-plugging rate. The filter-plugging rate was determined by measuring the time required to collect the initial sample filtered through the membrane and the time required to collect the second sample after 5 and 15 minutes of filtration. The SDI was calculated from the equation below:

$$SDI = \frac{1 - (t_f/t_i)}{\Delta t} 100 \tag{12}$$

where t_i is the time to collect initial 500 mL of sample, t_f the time to collect final 500 mL of sample, and Δt the total running time for the test.

The modified fouling index (MFI) test was also performed by recording the flux decline rate at 30 sec intervals over the filtration period. MFI was determined from a plot of filtration time per total permeate volume (t/V) *vs.* total filtrate volume (V) and its definition is as follows (8):

$$MFI = \frac{\alpha C_s \eta}{2\Delta P A^2} \tag{13}$$

where α is the specific cake resistance, C_s the bulk concentration of suspended solids, ΔP the transmembrane pressure, and A the area of the membrane used for the test.

MF and UF as NF Pretreatment

Microfiltration (MF) and ultrafiltration (UF) were tested as pretreatment methods for surface water NF. Tubular ceramic membranes (Techsep, France) having a zirconia skin layer were evaluated in a crossflow mode. The inner diameter of the membranes was 6 mm and the effect membrane

area was 0.01 m^2. Filtration was performed in inside-out mode. Details of the experimental setup were in ref (27). The NF feed was pretreated using MF and UF in a separate small-scale filtration device and transferred to the experimental apparatus for NF (off-line operation). Experiments using MF and UF were conducted at a crossflow velocity of 2.0 m/sec and in a concentration mode whereas NF experiments were carried out at 0.6 m/sec or 1.0 m/sec. The pretreatments were terminated after gathering 20 L of permeate which was used as the NF feed. Details on these pretreatment processes are given in Table 2.

Measurements of Various Flux

In this paper, the terms of initial water flux (J_w), final flux (J_f), flux after rinsing (J_r), and flux after manual cleaning (J_m) were used to characterize the membrane filtration performance. J_w is the water flux through clean membrane. Before the nanofiltration of raw water, the J_w value for each membrane was determined by the filtration of ultrapure water when a steady flux was reached. The feed tank and other flow lines were then emptied and filled with raw water. Nanofiltration was performed until the pseudo steady state was reached. The permeate flux at this moment is denoted as J_f. The feed tank and other flow lines are then emptied again and refilled with the ultrapure water. The surface rinsing of the tested membrane with ultrapure water continued for 10 min without applying transmembrane pressure. Then the rinsing water was then discarded. J_r is the flux determined by the ultrapure water immediately after the surface rinsing. Finally, J_m was measured in the same way after the membrane surface was cleaned manually with a sponge.

Analysis of Hydraulic Resistance

The resistance-in-series model was applied to evaluate the portion of each resistance of the total resistance. According to Choo and Lee (28) the

Table 2. Properties and operating conditions of the tubular membranes used in NF pretreatment

Type	Trade name	Pore size or MWCO[a]	Operating condition
Microfilter	Carbosep M45	0.45 μm	
	Carbosep M14	0.14 μm	2 m/sec, 0.2 bar
	Carbosep M6	0.08 μm	
Ultrafilter	Carbosep M3	MWCO[a] 150,000	2 m/sec, 1.0 bar
	Carbosep M8	MWCO[a] 50,000	2 m/sec, 2.0 bar

[a]Molecular weight cut off (in Dalton).

permeate flux (J) takes the following form:

$$J = \frac{\Delta P}{\eta R_t} = \frac{\Delta P}{\eta(R_m + R_p + R_{ef} + R_{if})} \tag{14}$$

where J is the permeate flux; ΔP the membrane pressure; η the viscosity of the permeate; R_t the total resistance; R_m the intrinsic membrane resistance; R_p the cake resistance; R_{ef} the external fouling resistance formed by irreversible surface deposition of solids on the membrane surface; and R_{if} the internal fouling resistance due to any irreversible adsorption/adhesion of small molecules. Each resistance value (R_m, R_p, R_{ef} and R_{if},) can be obtained and the experimentally determined flux, J_w, J_f, J_r and J_m.

$$R_m = \Delta P/(\eta \cdot J_w) \tag{15}$$

$$R_{if} = \Delta P/(\eta \cdot J_m) - \Delta P/(\eta \cdot J_w) \tag{16}$$

$$R_{ef} = \Delta P/(\eta \cdot J_r) - \Delta P/(\eta \cdot J_m) \tag{17}$$

$$R_p = \Delta P/(\eta \cdot J_f) - \Delta P/\Delta P(\eta \cdot J_r) \tag{18}$$

The R_{sa} is the resistance caused by solids deposition just on top of the membrane surface, which represents the extent of cake formation during filtration. This can be obtained simply by a summation of R_p and R_{ef}.

$$R_{sa} = R_p + R_{ef} \tag{19}$$

RESULTS AND DISCUSSION

Effect of Crossflow Velocity on Flux and Hydraulic Permeation Resistances

Figure 3 shows flux versus time behaviors during the crossflow nanofiltration of untreated raw water. At a lower fluid velocity of 0.7 m/sec, a rapid drop in flux was observed at the initial stage (within 50 hr) while only a gradual flux decline was observed at a higher fluid velocity of 1.0 m/sec.

To analyze the influence of fluid velocity on fouling layer characteristics, hydraulic resistances were evaluated using the resistance-in-series model. In Table 3, as the crossflow velocity was increased from 0.7 to 1.0 m/sec, even at a longer operation time the values for R_p and R_{ef} decreased by 33 % (30.9 $\rightarrow$ 20.6) and 20% (20.6 $\rightarrow$ 16.5), respectively. In both cases, R_{if} was negligible compared to other resistances which suggests that membrane fouling due to organic adsorption was less important than that due to particle deposition and cake formation.

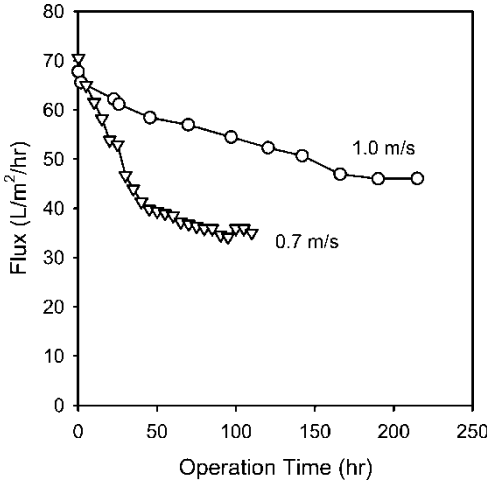

Figure 3. Permeate flux of NF with different crossflow velocities. Operating conditions: feed; untreated raw water, membrane; NF-45, transmembrane pressure; 10.0 bar. (▽: 0.7 m/s; ○: 1.0 m/s).

It is interesting to note that NOM such as humic and fulvic acid caused significant NF fouling in many cases (4, 5) while NOM was found to be less important for NF fouling in our study. This difference can be attributed to a low $SUVA_{254}$ value ($1.7\,L/mg^{-m}$) of the raw water in our case. Since the $SUVA_{254}$ represents the hydrophobicity of NOM in raw water, it is not surprising that the NOM adsorption would be less at lower $SUVA_{254}$. This result is in good agreement with the reports of Nilson and DiGiano (6) and Huber (29) who found that the hydrophilic NOM was less responsible for a decline in NF flux.

Table 3. Effect of crossflow velocity on each resistance in surface water nanofiltration. Operating condition: membrane; polypiperazine amide (NF-45, Filmtec), transmembrane pressure; 10 bar

Fluid Velocity, m/sec	Resistance, $10^{12}\,m^{-1}$	
	0.7	1.0
R_m	51.2 (49.8)	50.7 (57.7)
R_p	30.9 (30.0)	20.6 (23.4)
R_{ef}	20.6 (20.0)	16.5 (18.8)
R_{if}	0.2 (0.2)	0.1 (0.1)
R_t	102.9 (100.0)	87.9 (100.0)

Values in brackets is the percentage of each resistance of the total one.

Even though the flux decline was retarded with an increase in crossflow velocity, the R_{sa} $(=R_p + R_{ef})$ still remained an important component $(>42\%)$ of the overall hydraulic resistance, even at higher fluid velocity, indicating the significant role of particles and colloids deposition in flux loss. This result suggests that flux improvement may be achieved by eliminating particles and colloids in raw water using pretreatments like MF or UF.

Pretreatment Using Microfiltration and Ultrafiltration

NF performance was evaluated after raw water had undergone microfiltration (MF) or ultrafiltration (UF) pretreatment. Figure 4 (a) compares the NF flux under various pretreatment conditions at lower fluid velocity (0.7 m/sec). Flux improvement was observed when an MF/UF pretreatment was applied, and the extent of fouling was significantly lowered using a smaller pore size prefilter. After MF pretreatment, the flux loss continued to be important compared to UF pretreatment. For instance, NF flux decreased by $29\,L/m^2/hr$ and $18\,L/m^2/hr$ over a 90-hr period using 0.14 μm MF and 0.08 μm MF, respectively. On the other hand, NF flux declined by less than $7\,L/m^2/hr$ even after 110-hr of operation using UF pretreatments, which corresponds to 10% of the initial flux and almost negligible. In the case of a higher crossflow rate (1.0 m/sec) a similar fouling tendency was observed as shown in Fig. 4(b). These results indicate that NF foulants were efficiently rejected by UF and that their size is larger than the pore size of UF. According to previous studies (5), the size distribution of NOM (humic and fulvic acid) in surface water ranges from 1,000∼20,000, and, as a result, the rejection by UF is very low. Therefore, it appears that colloidal matters rather than NOM are likely to have a significant effect on NF membrane fouling. This result is consistent with the results reported by Chellam et al. (16) who concluded that NF fouling was controlled by colloidal material rather than NOM.

To further investigate the NF filtration characteristics and the role of MF/UF pretreatment, the hydraulic resistances for each experiment were determined using the Eqn (16) to (20) and are summarized in Table 4. The contribution of R_{if} to the total resistance, R_t was negligible, which also suggests that the flux loss was not relevant to the adsorption/precipitation of small molecules. R_p for MF pretreated water significantly decreased compared to untreated raw water. However, R_{ef} was not reduced to any extent for MF treatment, and, thus, the relative portion of R_{ef} became even higher than that for raw water in case of 0.14 μm MF prefiltration. On the contrary, both R_p and R_{ef} decreased in the case of UF pretreatment. This indicates that the flux improvement by MF was mainly due to a reduction in the polarization layer but that by UF was due to the reduction of both polarization and the external fouling layers.

Table 4 also indicates that a small portion of R_p still remains even after UF treatment. Clearly, it is not caused by inorganic salt deposition since the

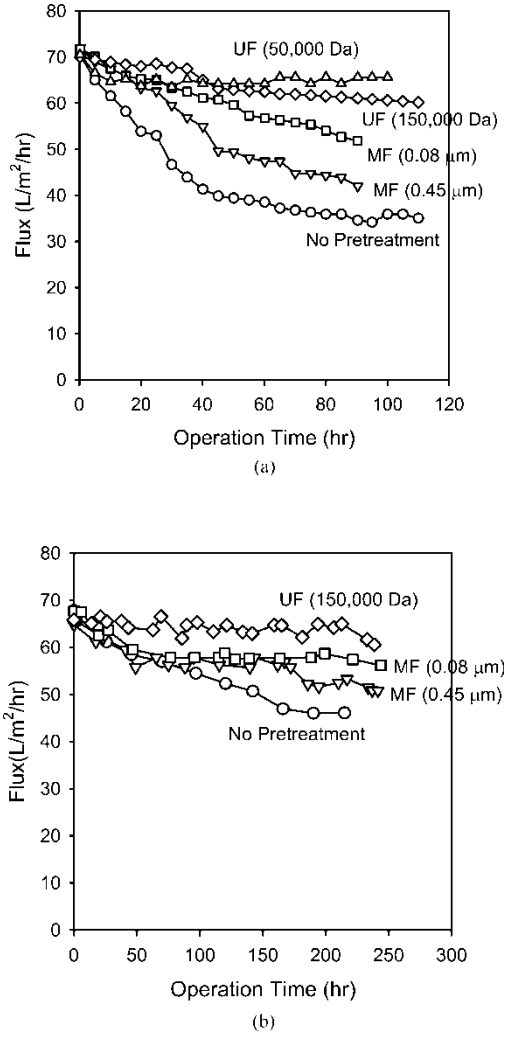

Figure 4. Comparison of flux variation during NF among different pretreatments. Operating conditions: membrane; NF-45, transmembrane pressure; 10.0 bar. (a) crossflow velocity of 0.7 m/sec (○: No pretreatment; ▽: MF (pore size: 0.45 μm); □: MF (pore size: 0.08 μm); ◇ : UF (MWCO: 150,000 Da); △: UF (MWCO: 50,000 Da). (b) crossflow velocity of 1.0 m/sec (○: No pretreatment; ▽: MF (pore size: 0.14 μm); □: MF (pore size: 0.08 μm); ◇ : UF (MWCO: 150,000 Da).

divalent ion concentration in feed water is small to cause scale formation. Instead, R_p after UF treatment may be attributed to the formation of reversible gel layer by small colloidal particles and dissolved organics that can pass through UF membranes. Nevertheless, R_p values after UF treatment are

Table 4. Resistances in nanofiltration in raw and pretreated water

		Low flow velocity (0.7 m/sec)			
		MF pretreatment		UF pretreatment	
	Without pretreatment	0.14 μm	0.08 μm	150,000 Da	50,000 Da
R_m	51.2 (49.8)	51.2 (60.2)	51.2 (73.4)	51.2 (83.0)	51.2 (91.7)
R_p	30.9 (30.0)	10.5 (12.4)	11.0 (15.8)	6.5 (10.5)	4.6 (8.3)
R_{ef}	20.6 (20.0)	23.0 (27.1)	7.1 (10.1)	4.0 (6.5)	0.0 (0.0)
R_{if}	0.2 (0.2)	0.3 (0.4)	0.5 (0.7)	0.0 (0.0)	0.0 (0.0)
R_t	102.9 (100.0)	85.0 (100.0)	69.8 (100.0)	61.7 (100.0)	55.8 (100.0)
		High flow velocity (1.0 m/sec)			
		MF pretreatment		UF pretreatment	
	Without pretreatment	0.45 μm	0.08 μm	150,000 Da	
R_m	50.7 (57.7)	51.1 (72.2)	54.0 (84.4)	53.2 (87.9)	
R_p	20.6 (23.4)	7.8 (11.1)	5.0 (7.8)	2.3 (3.8)	
R_{ef}	16.5 (18.8)	11.4 (16.1)	4.7 (7.3)	4.7 (7.7)	
R_{if}	0.1 (0.1)	0.4 (0.6)	0.3 (0.5)	0.3 (0.5)	
R_t	88.3 (100.0)	70.7 (100.0)	64.0 (100.0)	60.5 (100.0)	

Values in brackets is the percentage of each resistance of the total one.

only 10% $\sim$ 20% of those without pretreatment, suggesting that most foulants resulting in R_p appear to be removed by UF pretreatment.

This can be attributed to the characteristics of different size particles and their effect on resistances. While large particles tend to form a reversible polarization layer and represent the main cause of R_p, they can be easily removed by MF treatment. However, small particles, which are not easily detached from the membrane surface after deposition, would be expected to act as R_{ef}, rather than R_p. Thus, these small particles and colloids, which are able to pass through the pores of a microfilter, still remain and produce considerable R_{ef} after MF treatment. In UF, however, virtually all particles can be removed from the treated water and R_{ef} would be expected to decrease as well as R_p. This is discussed below.

Analysis of fouling index for pretreated water also presents the difference between MF and UF pretreatments (Table 5). The median turbidity following all MF/UF treatments was less than 0.1 NTU, whereas fouling indexes, i.e. SDI and MFI, were different for each treatment. For example, the SDI of raw water was 6.5, while those of treated water using 0.45, 0.14 and 0.08 μm MF were 4.66, 4.66 and 3.24, respectively. In the case of UF pretreatment, the value of SDI was too small value to be measured, which implies that nearly all particles and colloids were removed. A similar trend also can be seen in the MFI test results. This indicates that a considerable amount of colloids, the size of which is smaller than the pore size of MF, remained after MF pretreatment, even though their relative amount was small. The size of these particles may be smaller than the pore size of the membrane used for the SDI/MFI test, but these could still be detected in SDI/MFI test since they are able to aggregate near the membrane surface due to thermodynamic instability (30).

In Table 4 and 5, it is likely that R_p is related to SDI and MFI. After UF treatment, SDI and MFI became negligible and R_p is reduced significantly

Table 5. Water quality of pretreated raw water using MF/UF

Type	Pore size or MWCO[a]	SS (mg/L)	Turbidity (NTU)	SDI	MFI (s/L^2)
Without pretreatment		5.5	5.0	6.50	645.0
MF	0.45 μm	—[b]	<0.1	4.66	65.7
MF	0.14 μm	—[b]	<0.1	4.66	55.7
MF	0.08 μm	—[b]	<0.1	3.24	17.3
UF	MWCO[a] 150,000	—[b]	<0.1	0[b]	0[b]
UF	MWCO[a] 50,000	—[b]	<0.1	0[b]	0[b]

[a]Molecular weight cut off (in Dalton).
[b]Not detected.

(over 50%). This indicates that foulants resulting in R_p were mainly particles that were detected by SDI/MFI test. On the other hand, the foulants resulting in R_{ef} cannot be effectively determined by SDI/MFI test. For instance, comparing R_{ef} and SDI/MFI results in 0.08 MF and 150,000 Da UF treatments, R_{ef} did not change but SDI/MFI became zero. This suggests that SDI and MFI are not sensitive to detect the potential of external fouling.

It is noteworthy that the efficiency of pretreatment depends on the pore size of the prefilter. Since the particle distribution in pretreated water is determined by the prefilter pore size, the pretreatment efficiency can be expressed as a function of particle size in feed water. Thus, the hydrodynamic factors of particles and colloids in feed water, especially particle size, are of great importance in NF filterability.

Theoretical Analysis of MF/UF Pretreatment Efficiencies

Based on the previous experiments, the efficiency of MF/UF pretreatment depended on the size of particles in treated water. Thus, the particle deposition and fouling phenomena in the NF system were assessed with a theoretical approach to particle transport mechanisms to provide a quantitative evaluation for flux behavior and pretreatment efficiencies.

In Eqs. (3) to (7), particle transport is expressed as a function of hydrodynamic back transport and permeation drag (flux) because the diffusion coefficients, (D_B and D_S) are dependent on the particle radius, r_p. As described above, the net back-transport velocity of a particle is the sum of various velocity components, including Brownian diffusion, shear-induced diffusion, lateral migration. Figure 5 shows the profiles of the back-transport velocities with different particle sizes and fluid velocities, indicating the particle transport and deposition is greatly dependent on its size. With respect to the effect of fluid velocity, the larger the fluid velocity, the larger is the back-transport velocity. In addition, the net particle back-transport velocity exhibited a minimum at a particle diameter of approximately 0.2 μm.

In some cases, interaction-induced migration was found to be a major mechanism in determining particle back-transport in other recent studies (25). Nevertheless, the effect of interaction-induced migration on NF flux appeared be negligible in this work because of low surface potential in feed water used here. In the previous studies (23, 25) synthetic particles were used and the absolute zeta potential was above 40 mV. In this study, the absolute value was smaller than 10 mV, indicating that only negligible electrical repulsion and potential barrier occur.

The theoretical approach to particle transport mentioned above helps explain the relationship between the pore size of MF/UF used in the pretreatment and the steady state flux of NF. As shown in Fig. 5, a minimum of back transport velocity exists at a particle diameter of approximately 0.2 μm. Below this size, the smaller the particle diameter, the larger is particle back

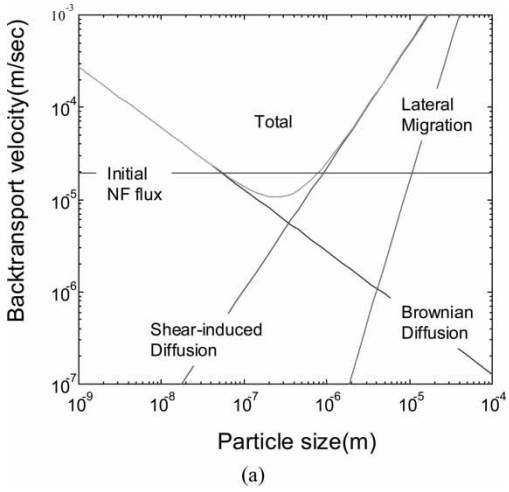

Figure 5. Profiles of the back-transport velocities based on models described in Eqn (4) to (9) as a function of particle diameter. (a) crossflow velocity of 0.7 m/sec ($\gamma_w = 2{,}800$), (b) crossflow velocity of 1.0 m/sec ($\gamma_w = 4{,}000$).

transport. Thus it can be hypothesized that the increase in flux by pretreatment is caused by the decrease in particle size in the treated water, assuming that all particles larger than the pore size of the prefilter are removed by pretreatment. Accordingly the steady state flux would be determined by the minimum value of particle back transport velocity in the treated water. When the minimum particle back transport in the treated water exceeds the initial permeation

velocity (water flux), however, no fouling would occur because the particle deposition should be negligible.

To further verify this relationship, the theoretical steady state flux calculated based on a hydrodynamic approach was compared with the experimental results. The pore size of the UF membrane was calculated from nominal *MWCO* value using the following Equation (31).

$$d_p = 0.147 \times 10^{-3} \times (MWCO)^{1/3} \tag{20}$$

where d_p is the pore size of the UF membrane.

Using the Eqs. (4) to (7), the dependence of permeate flux on the pore size of prefilter was calculated as shown in Fig. 6. Flux is initially constant under small pore size conditions because the flux cannot exceed the pure water flux. Then, flux decreases with the increasing pore size of prefilter. Finally, flux becomes constant again at large pore sizes because the backtransport velocity was minimum at particle size of 0.2 μm. This prediction is in good agreement with the experimental results, indicating that the quantitative prediction of MF/UF prefilter efficiency is possible through a hydrodynamic approach. The difference between the predicted and experimental flux may also result from the difference between nominal and effective pore size and the distribution of pore size.

The changes of R_p and R_{ef} can also be explained in the same way. Since particles with smaller back-transport velocity have higher a value for net velocity toward the membrane surface, it could be hypothesized that these particles could get much closer. A subsequent strong attachment of particles may cause irreversible hydraulic resistance of the cake layer that should be expressed as R_{ef}. As shown in Table 4, the R_p values in MF treatment (pore size of 0.45 and 0.14 μm) significantly decreased compared with those of untreated raw water. This can be attributed to the fact that particles with a larger back-transport velocity were removed by MF, since particles larger than 0.2 μm have a larger back-transport velocity as their size increases. However, the R_{ef} values were relatively unchanged after MF treatment, suggesting that particles with smaller back-transport still remained. With respect to MF of 0.08 μm and the UF pretreatment, however, the portion of R_{ef} was significantly reduced since the particles having smallest back-transport velocity, the size of which is around 0.2 μm, were also rejected through these prefilters.

Comparison of Specific Energy Consumption

Although the NF flux can be more improved with an smaller prefilter pore size, care should be taken in the selection of prefilters since the cost of pretreatment also increases with decreasing pore size. Thus the efficiency of MF/UF pretreatment was examined by considering the specific energy input into

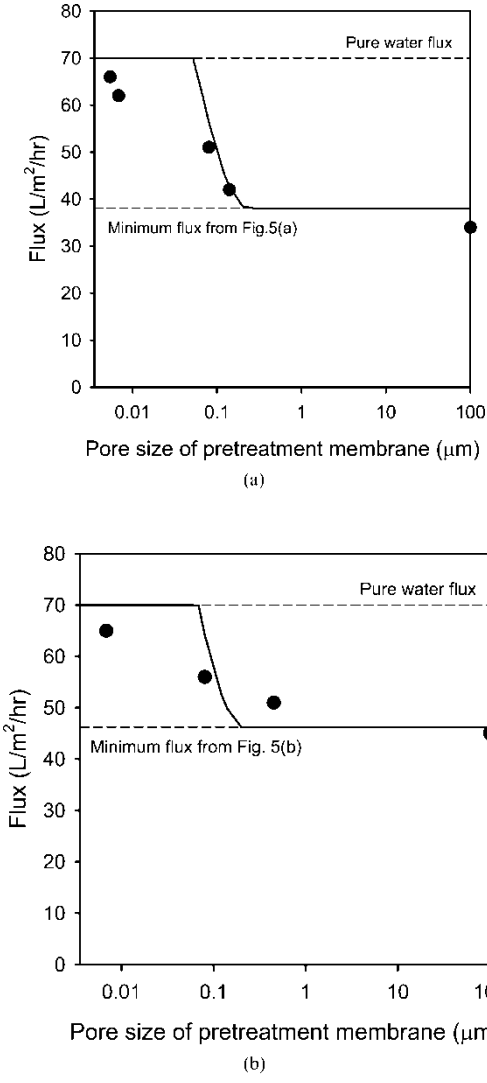

Figure 6. Comparison of theoretical and experimental steady-state flux during NF. The pore size of UF was estimated from Eqn (22). The filled symbols correspond to the experimental results. (a) crossflow velocity of 0.7 m/sec ($\gamma_w = 2{,}800$), (b) crossflow velocity of 1.0 m/sec ($\gamma_w = 4{,}000$).

each system to determine the optimum pretreatment conditions in terms of energy utilization.

Table 6 compares the permeability of MF/UF pretreatments. As expected, the smaller the pore size of membrane pretreatment is, the smaller the permeability occurs, and the more the transmembrane pressure is

Table 6. Comparison of MF/UF permeability during pretreatment

Type	Pore size or MWCO[a]	Operating condition	Pure water permeability (L/m^2-hr-bar)	Average permeability[b] (L/m^2-hr-bar)
MF	0.45 μm	0.2 bar, 2 m/sec	1400	387.0
MF	0.14 μm	0.2 bar, 2 m/sec	750	300.5
MF	0.08 μm	0.2 bar, 2 m/sec	465	154.5
UF	MWCO[a] 150,000	1.0 Bar, 2 m/sec	200	57.2
UF	MWCO[a] 50,000	2.0 Bar, 2 m/sec	119	49.6

[a]Molecular weight cut off (in Dalton).
[b]Average permeability over the time to produce 20 L pretreated raw water.

needed. However, the average permeability during the filtration of raw water showed a much smaller value from the permeability of pure, suggesting that potential foulants, which could cause NF flux loss, were retained and deposited on the MF/UF prefilter.

Figure 7 illustrates the final permeate flux at the end of the NF operation as a function of specific energy input to MF/UF pretreatment. The specific energy input to the pretreatment was calculated using Eqn (10) and the filtration data over the time to produce 20 L of pretreated water. In both fluid conditions, the improvement in flux as the result of pretreatment was not linearly proportional to the energy input to pretreatment step. As discussed above, the back-transport velocity of particles smaller than 0.2 μm becomes larger as the size of particle decreases. Below this size, the NF flux could not be improved significantly,

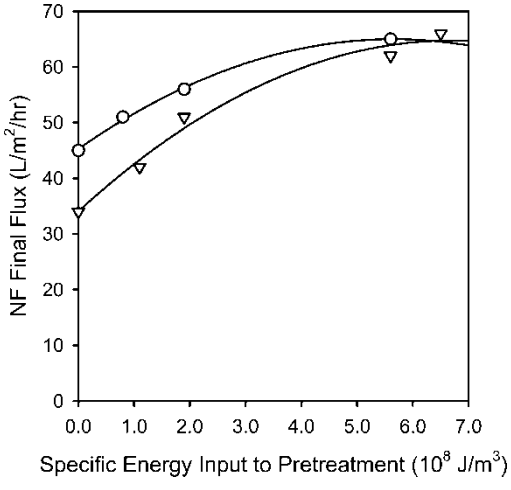

Figure 7. Improvement of NF flux by MF/UF pretreatment as a function of specific energy input to pretreatment step (▽: 0.7 m/s; ○: 1.0 m/s).

even though the MF/UF membrane of smaller pore size is applied and the average particle size of the feed solution decreases. These data also indicates that there will be an optimum pore size of MF/UF exists for obtaining high NF flux in terms of energy efficiency.

Figure 8 shows the specific energy input to NF, pretreatment and the total as calculated from Eq. (13). It can be seen that the smaller the pore size of membrane pretreatment is, the smaller is the specific energy input to the NF

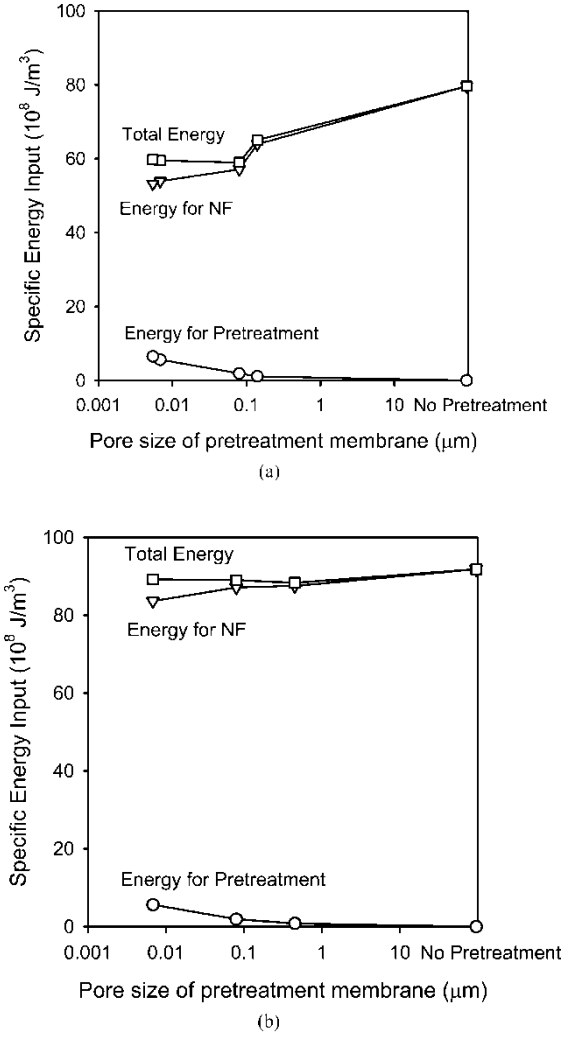

Figure 8. Variations of specific energy input with different pore size of pretreatment membrane (○: Energy for pretreatment; ▽: Energy for NF; □: Total energy consumption). (a) crossflow velocity of 0.7 m/sec, (b) crossflow velocity of 1.0 m/sec.

process, but the larger the specific energy input to the pretreatment step. Thus the total specific energy consumed by both NF and pretreatment reaches a minimum value for certain prefilter pore size: 0.08 μm MF under low crossflow conditions and 0.45 μm MF under high crossflow conditions, respectively.

Therefore, the following suggestions can be proposed for the optimal pretreatment based on the energy consumption considerations: if the pore size of the prefilter is too large to retain small colloids, the NF flux decreases with time and it becomes necessary to spend a considerable amount of energy to produce same volume of permeate. On the other hand, flux may not decreased, excessive energy should be needed for pretreatment if the pore size of prefilter is too small. Consequently, the pore size of the prefilter should be determined at the point where the specific energy consumption is minimized for efficient pretreatment.

CONCLUSIONS

In this work, the efficiency of pretreatments using MF/UF to mitigate NF membrane fouling was investigated under various conditions. The following conclusions were withdrawn:

1) An analysis of hydraulic resistance indicated that flux loss in NF was attributed to the deposition of small colloids rather than adsorption of dissolved organic matter (DOM). This is because the feed water used in this study contains low amounts of hydrophilic organics (DOC less than 2 mg/L; SUVA less than 2 L/mg-m). Hydraulic resistances in NF decreased with an increase in fluid velocity but cake resistance including polarization and external fouling resistances were still substantial.
2) Pretreatment of raw water using MF/UF was attempted to improve NF flux and mitigate membrane fouling. The NF flux increased with decreasing nominal pore size of the prefilter, suggesting that the size of particles in treated water greatly affects the NF flux.
3) NF flux loss and pretreatment efficiency were quantitatively interpreted by employing a theoretical approach based on the particle back-transport model. The steady-state flux at a given pore size of prefilter can be predicted based on this model. The changes in hydraulic resistances under different pretreatment conditions can also be explained.
4) Considering the specific energy consumed by MF/UF pretreatment and NF process, optimum pretreatment condition were explored in terms of pore size of prefilter. Total specific energy consumption shows the minimum value in a pore size of prefilter, presenting that the pretreatment using MF/UF should be chosen in terms of energy utilization efficiency.

REFERENCES

1. Spangenberg, C.W., Kalinsky, A., Akiyoshi, E., and Lozier, J.C. (Feb. 23–26, 1997) Selection, evaluation and optimization of organic selective membranes for color and DBP precursors removal, *Proceedings of AWWA Membrane Technology Conference*, New Orleans, LA, USA; 537–579.
2. Yasumoto, M., Shoichi, K., and Masaki, Itoh (1998) Advanced membrane technology for application to water treatment. *Wat. Sci. Tech.*, 37 (10): 91–99.
3. Scott, D.N., Freeman, P.E., and Crook, J. (Aug. 13–16, 1995) An update on membrane water reuse projects, *Proceedings of AWWA Membrane Technology Conference*, Reno, Nevada, USA; 665–697.
4. Allgeier, S.C. and Summers, R.S. (Aug. 13–16, 1995) Effect of Mass Transfer Resistance and System Recovery on Membrane Permeation, *Proceedings of AWWA Membrane Technology Conference*, Reno, Nevada, USA; 39–66.
5. Jucker, C. and Clark, M.M. (1995) Adsorption of aquatic humic substances on hydrophobic ultrafiltration membranes. *J. Membrane Sci.*, 96: 137–52.
6. Nilson, J.A. and DiGiano, F.A. (1996) Influence of NOM composition on nanofiltration. *J. AWWA*, 88 (5): 53–66.
7. Yoon, S.H., Lee, C.H., Kim, K.J., and Fane, A.G. (1998) Effect of calcium ion on the fouling of nanofilter by humic acid in drinking water production. *Wat. Res*, 32 (7): 2180–2186.
8. Mallevialle, J., Odendaal, P.E., and Wiesner, M.R. (1996) *Water Treatment Membrane Processes*; McGraw-Hill: New York.
9. Champlin, T. and Hendricks, D. (1995) Pilot testing NF membranes for direct treatment of low-turbidity surface waters, Proceedings of AWWA Membrane Technology Conference, Reno, Nevada, USA, August 13–16; 229–250.
10. Zhu, Xiaohua, Hong, S., Childress, A.E., and Elimelech, M. (Aug. 13–16, 1995) Colloidal fouling of reverse osmosis membranes: Experimental results, fouling mechanisms, and implications for water treatment, *Proceedings of AWWA Membrane Technology Conference*, Reno, Nevada, USA; 251–263.
11. Gusses, A.M., Speth, T.F., Allgeier, S.C., and Summers, R.S. (Feb. 23–26, 1997) Evaluation of surface water pretreatment processes using the rapid bench-scale membrane test, *Proceedings of AWWA Membrane Technology Conference*, New Orleans, LA, USA; 765–782.
12. Hoek, J.P. and Bonné, P.A.C. (Aug. 13–16, 1995) Application of hyperfiltration at the amsterdam waterworks: Effect of pretreatment on operation and performance, *Proceedings of AWWA Membrane Technology Conference*, Reno, Nevada, USA; 277–294.
13. Lebeau, T., Lelievre, C., and Buisson, H. (1998) Immersed membrane filtration for the production of drinking water: Combination with PAC for NOM and SOCs removal. *Desalination*, 117: 219–231.
14. Hassan, A.M., Abanmy, A., and Farooque, A.M. (Nov. 18–24, 1995) Quantitative determination of polymeric scale inhibitors by polyelectrolyte titration, *IDA World Congress on Desalination and Water Sciences*, Abudabi, 115–129.
15. Braghetta, A., Hotaling, M.L., Vickers, J., Jjacangelo, J., and Utne, B. (Feb. 23–26, 1997) Impact of DAF pretreatment of a surface water with microfiltration and ultrafiltration: Performance and estimated cost, *Proceedings of AWWA Membrane Technology Conference*, New Orleans, LA, USA; 1221–1236.
16. Chellam, S., Jacangelo, J.G., Bonacquisti, T.P., and Schauer, B.A. (1997) Effect of pretreatment on surface water nanofiltraiton. *J.AWWA*, 89 (10): 77–89.

17. Ericsson, B. and Hallmans, B. (1991) Membrane filtration as a pre-treatment method. *Desalination*, 82: 249–260.
18. Lozier, J.C., Jones, G., and Bellamy, W. (1997) Integrated membrane treatment in Alaska. *J.AWWA*, 89 (10): 50–64.
19. Morris, K. and Taylor, J. (Aug. 13–16, 1991) DBP Precursor Removal by Reverse Osmosis, *Proceedings of AWWA Membrane Technology Conference*, Orlando, FL, USA; 563–570.
20. Olivieri, V.P., Parker, D.Y., Jr., Willinghan, G.A., and Vickers, J.C. (Aug. 13–16, 1991) Continuous Microfiltration of Surface Water, *Proceedings of AWWA Membrane Technology Conference*, Orlando, FL, USA; 563–570.
21. Clair, D.H., Adams, P.V., and Shreve, S. (Feb. 23–26, 1997) Microfiltration of a high-turbidity surface water with post-treatment by nanofiltration and reverse osmosis, *Proceedings of AWWA Membrane Technology Conference*, New Orleans, LA, USA; 233–268.
22. Belfort, G., Davis, R.H., and Zydney, A.L. (1994) The behavior of suspensions and macrimolecular solutions in crossflow microfiltration. *J. Membrane Sci.*, 96: 1–58.
23. Bacchin, P., Aimar, P., and Sanchez, V. (1995) Model for colloidal fouling of membranes. *AIChE J.*, 41 (2): 368–376.
24. Drew, D.A., Schonberg, J.A., and Belfort, G. (1991) Lateral inertial migration of a small sphere in fast laminar flow through a membrane duct. *Chem. Eng. Sci.*, 46: 3219–3224.
25. Yoon, S.H., Lee, C.H., Kim, K.J., and Fane, A.G. (1999) Three-dimensional simulation of the deposition of multi-dispersed charged particles and prediction of resulting flux during cross-flow microfiltration. *J. Membrane Sci.*, 161: 7–20.
26. APHP; AWWA. (1995) *WEF. Standard Methods for the Examination of Water and Wastewater*, 18th edn; Am. Public Health Assoc.: Washington, D.C..
27. Kim, J.H., Choo, K.-H., and Yi, H.S. (2001) Effect of membrane support material on permeability in the microfiltration of brining wastewater. *Desalination*, 140 (1): 55–65.
28. Choo, K.H. and Lee, C.H. (1998) Hydrodynamic behavior of anaerobic biosolids during crossflow filtration in the membrane anaerobic bioreactor. *Wat. Res.*, 32 (11): 3387–3397.
29. Huber, S.A. (1998) Evidence for membrane fouling by specific TOC constituents. *Desalination*, 119: 229–234.
30. Harmant, P. and Aimar, P. (1998) Coagulation of colloids in a boundary layer during crossflow filtration. *Colloids and Surfaces A*, 138: 217–230.
31. Sethi, S. and Wiesner, M. (1991) *Computer Simulation Model for Performance and Cost Modeling of Ultrafiltration and Microfiltration*; Rice University.